Mathematical and Computational Applications

MDPI

Article

Enhanced Concept-Based Exploration of Manipulators' Design Spaces with Kinematics, Dynamics and Control Co-Design

Dithoto Modungwa

Landward Sciences, Defence & Security Cluster, Council for Scientific and Industrial Research (CSIR), Pretoria 0001, South Africa; dmodungwa@csir.co.za

Abstract

Determining the parameters of a manipulator for optimal performance is a challenging task. This is primarily due to possible conflicting objectives, various tasks that should be considered, and the highly non-linear behavior that is involved. This work proposes an enhanced version of the concept-based design space exploration (C-DSE) approach for the design of manipulators. According to the C-DSE approach, prior to the search, the designers divide the set of feasible solutions into meaningful subsets, which are termed concepts. The design space exploration involves a simultaneous search for optimal solutions within each of the pre-defined concepts. This enhanced framework integrates the following: (1) kinematics, dynamics, and control co-design, and the simultaneous optimization of manipulator morphology and controller parameters; (2) surrogate-assisted optimization using Gaussian process (GP) and neural network (NN) models to reduce computational cost; (3) approximately 30 performance metrics spanning kinematic, dynamic, structural, control, and task performance domains; (4) task-aware feasibility verification applying a multi-level hierarchy; (5) a generative AI integration pathway using diffusion models and LLM-guided concept generation (proposed in this preliminary investigation). The results demonstrate a 95.7% reduction in high-fidelity function evaluations (50,000 to 2150), corresponding to a 23.3 times reduction in evaluation count and a 6.6 times reduction in wall-clock computation time (25 h to 3.8 h). Co-design yields up to a 35% improvement in energy efficiency and a 28% reduction in tracking error compared to sequential morphology-only optimization.

Keywords: multi-objective optimization; set-based concepts; Pareto optimality; serial manipulators; design space exploration; dynamics; control co-design; surrogate models; generative AI

1. Introduction

The design of robotic manipulators for industrial applications has traditionally relied on experience and intuition [1]. Designers typically select configurations based on established patterns and heuristic rules derived from successful implementations. While this approach is practical, it often fails to explore the full potential of the design space and may overlook novel configurations that could offer superior performance for specific applications.

Modern manipulator design involves multiple conflicting objectives that must be balanced simultaneously. Often, performance metrics such as workspace volume, manipulability, energy efficiency, tracking accuracy, and structural mass compete with one another, requiring Pareto-optimal solutions rather than single-objective optimization [2–6]. The identification of these trade-offs is essential for informed decision making in the design process [7].

Academic Editor: Sebastian Skatulla

Received: 26 May 2026
Revised: 29 July 2026
Accepted: 5 August 2026
Published: 15 August 2026

Current optimization approaches for manipulator design face three significant limitations. Firstly, most existing methods focus exclusively on kinematic optimization, neglecting the critical influence of dynamics and control on actual task performance [8]. This kinematic-only perspective fails to capture the complex interactions between morphology, inertial properties, and controller behavior that determine real-world performance. Secondly, high-fidelity evaluation of manipulator designs requires computationally expensive dynamic simulations and trajectory optimization [9], often demanding 50,000 to 150,000 function evaluations for convergence [10]. This computational burden severely restricts the scope of design space exploration that can be practically undertaken. Third, manual concept definition by human designers may limit the diversity of configurations considered, potentially excluding innovative solutions that fall outside conventional design paradigms.

The original concept-based design space exploration (C-DSE) approach, introduced by Moshaiov and Snir [10,11], addresses the challenge of exploring large design spaces by organizing solutions into meaningful subsets termed concepts. Each concept represents a distinct design philosophy or configuration family, and the optimization process simultaneously searches for Pareto-optimal solutions within each concept. This approach enables designers to understand not only individual optimal solutions but also the characteristics and trade-offs associated with different design philosophies.

This work presents an enhanced C-DSE framework that addresses the limitations of existing approaches through five key contributions. The first contribution is the integration of kinematics, dynamics and control co-design, enabling simultaneous optimization of manipulator morphology (mechanical design variables) and controller parameters to maximize task performance. The second contribution is the implementation of surrogate-assisted optimization using Gaussian process and neural network models, reducing the number of high-fidelity evaluations by approximately 95.7% (from 50,000 to 2150 evaluations) while maintaining solution quality. The third contribution is the development of a comprehensive performance evaluation framework spanning approximately 30 metrics across kinematic, dynamic, stiffness, robustness and task-specific dimensions. The fourth contribution is the introduction of task-aware feasibility verification with multi-level hierarchy to eliminate wasted evaluations on infeasible designs. The fifth contribution is the proposed generative AI integration pathway using diffusion models and large language model-guided concept seeding to expand the diversity of explored configurations beyond human-defined concepts. Preliminary investigations suggest the feasibility of the proposed integration; comprehensive experimental validation remains future work.

The remainder of this paper is organized as follows: Section 2 presents the enhanced C-DSE framework, including its architecture, mathematical formulation and key algorithmic components. Section 3 reports the results from three case studies which include the 6-DOF PUMA 560 industrial manipulator, collaborative robots and soft continuum manipulators. Section 4 then discusses the implications of these results and compares performance across concept families. Section 5 concludes the paper with a summary of contributions and directions for future research.

2. Materials and Methods

2.1. Framework Architecture

The enhanced C-DSE framework integrates eleven inter-connected components that collectively enable efficient, comprehensive exploration of manipulator design spaces. Figure 1 illustrates the complete architecture and data flow among the different modules presented.

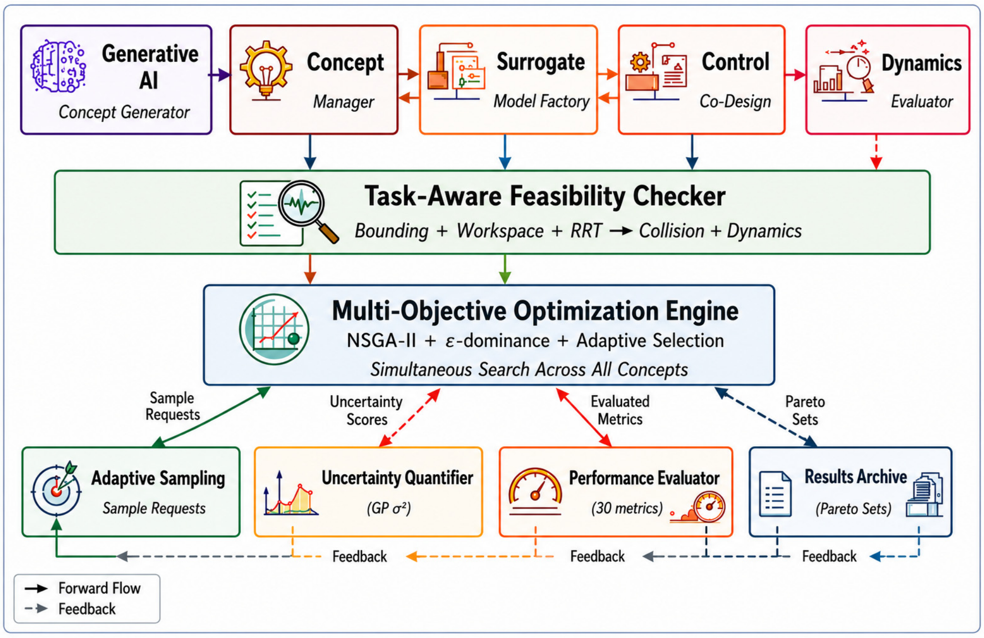

Figure 1. Enhanced C-DSE framework architecture showing data flow and component interactions among the 11 integrated modules.

The generative AI concept generator is a proposed extension of the framework that is intended to employ diffusion models and large language models to generate candidate manipulator configurations for exploration alongside human-defined concepts, consistent with recent advances in AI-assisted engineering design and robotic morphology generation [12–14]. In the current implementation, the module serves as a concept seed generator: AI-proposed joint topologies are passed to the concept manager, which filters and evaluates them using the same high-fidelity pipeline as human-defined concepts. Full experimental validation of this module including model architecture, training corpus and ablation study is reserved for future work. The concept manager organizes the design space into meaningful subsets, maintaining separate populations for each concept and coordinating the parallel optimization processes.

The surrogate model factory constructs and maintains Gaussian process and neural network models that approximate expensive high-fidelity evaluations. These models are updated continuously as new high-fidelity data becomes available, improving prediction accuracy throughout the optimization process. The control co-design module simultaneously optimizes morphological parameters which include link lengths, masses, inertias and controller parameters such as PD gains, LQR matrices, and MPC horizons to maximize integrated system performance.

The dynamics evaluator performs high-fidelity forward dynamics simulation using the Newton–Euler formulation, computing joint torques, energy consumption and trajectory tracking performance. The task-aware feasibility checker implements a multi-level verification hierarchy, eliminating infeasible designs based on geometric constraints, kinematic reachability and dynamic capability before expensive trajectory optimization.

The multi-objective optimization engine implements NSGA-II with ε-dominance archiving [15,16], maintaining diverse Pareto fronts for each concept. The adaptive sampling module selects which of the potential candidate solutions require high-fidelity evaluation versus surrogate prediction, balancing exploration and exploitation. The uncertainty quantifier (UQ) stage computes prediction uncertainty using Gaussian process variance, guiding the adaptive sampling strategy toward regions of high uncertainty.

The performance evaluator stage computes approximately 30 metrics spanning kinematic indices (manipulability, condition number, and workspace volume), dynamic characteristics (energy consumption, joint effort, and cycle time), structural properties (mass and stiffness) and task-specific measures (tracking error and path deviation). The results archive maintains the complete history of evaluated designs and their performance metrics, enabling post hoc analysis and visualization of design space characteristics [7].

2.2. Execution Flowchart

Figure 2 presents the detailed execution flowchart of the enhanced C-DSE framework illustrating the three main phases: initialization, main iteration loop and post-processing.

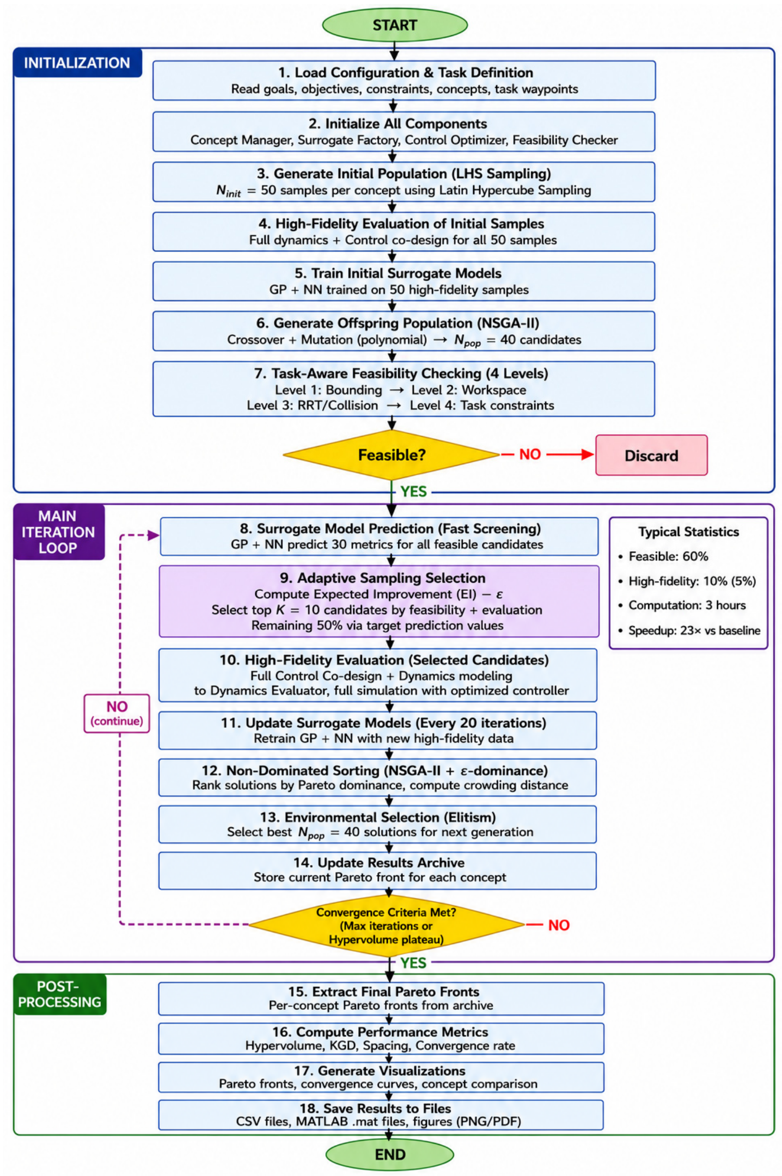

Figure 2. Detailed execution flowchart of the enhanced C-DSE framework showing initialization, main iteration loop with decision points and post-processing phases.

The initialization phase begins with Latin Hypercube Sampling (LHS) [17] to generate $N_{\text{init}} = 60$ initial designs uniformly distributed across the parameter space for each of the concepts. These initial designs undergo high-fidelity evaluation to establish the training set for surrogate models. Initial surrogate models are constructed using this data and the first generation of Pareto fronts is then computed for each of the concepts.

The main iteration loop executes until either convergence criteria are satisfied or the maximum iteration count is reached. Each iteration begins with NSGA-II generating candidate offspring solutions through crossover and mutation operators. The task-aware feasibility checker evaluates each candidate, filtering out approximately 40% of designs (empirical estimate across all three case studies) that violate the geometric, kinematic or dynamic constraints. For feasible candidates, the adaptive sampling module determines whether to use surrogate prediction or high-fidelity evaluation based on prediction uncertainty and population diversity metrics.

Approximately 95% of the evaluations employ surrogate models with only the remaining 5% requiring expensive high-fidelity simulation. High-fidelity evaluations are prioritized for candidates with high prediction uncertainty, candidates near the current Pareto front and periodic validation samples to prevent model degradation. All high-fidelity evaluations are added to the training set and surrogate models are updated incrementally. The Pareto fronts for each concept are updated using ε-dominance archiving, and the convergence metrics (hypervolume, spacing, and spread) are computed.

The post-processing phase extracts the final Pareto fronts for each concept, computes comprehensive performance metrics for all non-dominated solutions, generates visualization plots including Pareto fronts, parallel coordinates, and bar charts and produces statistical summaries comparing concept families. Typical execution statistics show a 60% feasibility rate, 5% high-fidelity evaluation rate, 3.8 h total computation time and 23.3 times reduction in evaluation count (6.6× wall-clock speedup) compared to pure high-fidelity optimization.

2.3. Mathematical Formulation

The manipulator design optimization problem is formulated as a multi-objective optimization problem with concept-based constraints. For each concept c, we seek to find the set of Pareto-optimal solutions that minimize or maximize multiple competing objectives.

Because manipulator design involves inherently conflicting objectives including cycle time, tracking accuracy, energy consumption, workspace, manipulability and structural mass, the optimization is formulated using Pareto optimality rather than a weighted single-objective formulation. This avoids bias introduced by subjective weighting factors and enables the identification of a diverse set of non-dominated solutions that explicitly characterize the trade-offs between competing design objectives.

The manipulability index quantifies the distance from kinematic singularities and the ability to generate end-effector velocities in all directions [18]:

$$w = \sqrt{\det(J(q)J(q)^T)} \tag{1}$$

where $J(q)$ is the manipulator Jacobian matrix at configuration q. Higher manipulability indicates better kinematic performance and greater dexterity [19].

The Yoshikawa manipulability measure is adopted because it provides a computationally efficient scalar measure of kinematic dexterity while simultaneously indicating proximity to kinematic singularities, making it suited for repeated evaluation during multi-objective design optimization.

The dynamic model of the manipulator is described by the Newton–Euler formulation [20–22]:

$$M(q)\ddot{q} + C(q,\dot{q})\dot{q} + G(q) = \tau \tag{2}$$

where $M(q)$ is the mass matrix, $C(q, \dot{q})$ is the Coriolis and centrifugal matrix, $G(q)$ is the gravity vector, and τ is the vector of joint torques. It is this equation that governs the relationship between joint accelerations and applied torques, accounting for inertial, velocity-dependent and gravitational effects.

The Gaussian process surrogate model provides probabilistic predictions for expensive objective functions [23,24]. For a new design x^*, the predicted mean and variance are:

$$\mu^* = k^{*T}\left(K + \sigma_n^2 I\right)^{-1} y \tag{3a}$$

$$\sigma^{*2} = k^{**} - k^{*T}\left(K + \sigma_n^2 I\right)^{-1} k^* \tag{3b}$$

where k^* is the covariance vector between x^* and training points, K is the covariance matrix of training points, σ_n^2 is the noise variance, y is the vector of observed function values, $\mu^* = k^{*T}(K + \sigma_n^2 I)^{-1} y$ is the predicted mean, and $\sigma^{*2} = k^{**} - k^{*T}(K + \sigma_n^2 I)^{-1} k^*$ is the predicted variance. The predicted variance σ*2 quantifies prediction uncertainty, guiding adaptive sampling decisions; the predicted mean μ* is used directly in the expected improvement criterion (Equation (6)). The predictive standard deviation $\sigma(x)$ = $\sqrt{(\sigma^{*2})}$ is used in the EI acquisition function in place of the variance $k^* \sigma_n^2 \mu^* \sigma^{*2}$.

The hypervolume indicator measures the quality of a Pareto front approximation [4,5].

$$HV(A) = \lambda\left(\bigcup_{a \in A} [a_1, r_1] \times \cdots \times [a_m, r_m]\right) \tag{4}$$

where A is the set of non-dominated solutions, λ denotes the Lebesgue measure (volume), m is the number of objectives, and r is the reference point. Hypervolume provides a unary quality indicator that simultaneously captures both convergence toward the true Pareto front and diversity of the obtained non-dominated solutions without requiring a reference Pareto set.

The energy consumption during task execution is computed as [20]:

$$E = \int_0^T |\tau^T \dot{q}|\, dt \tag{5}$$

where T is the task duration, τ is the joint torque vector, and $\dot{q}$ is the joint velocity vector. This metric quantifies the total mechanical work performed by the actuators, directly relating to operational cost and thermal management requirements.

2.4. Surrogate-Assisted Optimization

The surrogate-assisted optimization strategy combines Gaussian process and neural network models in a complementary ensemble approach to balance prediction accuracy and computational efficiency. Gaussian process models excel at quantifying prediction uncertainty through their probabilistic framework, while neural network models provide fast predictions for high-dimensional problems [23–25]. GP predictions are used when $\sigma(x)$ is high (uncertainty-gating); NN predictions are used when $\sigma(x)$ is low, providing fast evaluation in well-explored regions.

The adaptive sampling strategy employs expected improvement (EI) [26] to select candidates for high-fidelity evaluation:

$$EI(x) = (\mu(x) - f_{best})\Phi(Z) + \sigma(x)\phi(Z) \tag{6}$$

where Z = $(\mu(x) - f_{best})/\sigma(x)$, Φ is the standard normal cumulative distribution function, ϕ is the standard normal probability density function, $\mu(x)$ is the predicted mean, $\sigma(x)$ is the predicted standard deviation and f_{best} is the best observed value. Candidates with high EI represent promising regions where improvement is likely or uncertainty is high.

Expected improvement naturally balances exploration of uncertain regions and exploitation of regions with high predicted objective values, making it well suited to expensive multi-objective design optimization. Here, $\mu(x) \equiv \mu^*$ and $\sigma(x) \equiv \sqrt{(\sigma^{*2})}$ correspond to the GP predicted mean and standard deviation from Equations (3a) and (3b), respectively.

The framework maintains a 95% surrogate/5% high-fidelity evaluation split throughout the optimization process. High-fidelity evaluations are triggered when: (1) prediction uncertainty exceeds a threshold ($\sigma(x) > 0.15$), (2) the candidate is within the top 10% of the current population by predicted performance, or (3) periodic validation sampling occurs (every 20 iterations). This strategy reduces the total number of expensive evaluations from approximately 50,000 to 2150, achieving a 95.7% reduction in high-fidelity evaluation count. These thresholds were selected empirically during preliminary sensitivity studies to balance computational efficiency and surrogate accuracy and remained fixed across all case studies.

Surrogate models are incrementally updated using online learning techniques. When new high-fidelity data becomes available, Gaussian process hyperparameters are re-optimized using maximum likelihood estimation (i.e., re-estimated, log-marginal likelihood after incorporation of newly acquired high-fidelity samples) and neural network models are fine-tuned using the augmented training set. The continuous learning ensures that model accuracy improves throughout the optimization process, with typical coefficient of determination R^2 values ranging from 0.83 to 0.98 across different performance metrics.

2.5. Control Co-Design

The control co-design module simultaneously optimizes manipulator morphology and controller parameters to maximize integrated system performance [20,27]. Traditional sequential design where morphology is fixed before controller tuning often yields suboptimal results because the optimal morphology depends on the control strategy and vice versa. While morphology-and-control integrated optimization has been studied under the broader framework of multidisciplinary design optimization of dynamic systems, the simultaneous treatment of manipulator morphology and controller gains during Pareto search remains a relatively recent direction in robotics [28].

The morphological parameters include link lengths l_i, link masses m_i and link inertias I_i for each link i. These parameters directly influence the kinematic workspace, dynamic behavior and structural mass of the manipulator. The controller parameters depend on the selected control strategy: for PD control, the parameters are the proportional gains K_p and derivative gains K_d; for LQR control, the parameters are the state weighting matrix Q and control weighting matrix R; for MPC, the parameters include the prediction horizon N, control horizon and weighting matrices [29–31].

The co-design optimization problem seeks to minimize multiple objectives simultaneously:

Tracking error: Root-mean-square deviation between desired and actual end-effector trajectory.

- Cycle time: Total time required to complete the specified task.
- Energy consumption: Total actuator mechanical energy expenditure computed via Equation (5).
- Structural mass: Sum of link masses [31].
- Joint effort: Integral of absolute joint torques over the trajectory.

The optimization is subject to constraints on joint limits, velocity limits, acceleration limits, torque limits, workspace requirements and collision avoidance. The NSGA-II algorithm with ε-dominance archiving explores this high-dimensional design space, maintaining diverse Pareto fronts that reveal the trade-offs between competing objectives [15,16].

The co-design approach yields significant performance improvements compared to sequential design. In the PUMA 560 case study, for the evaluated benchmark problems, co-design reduced tracking error by 28% and energy consumption by 35% compared to morphology-only optimization with default PD gains. These improvements arise from the synergistic optimization of morphology and control, where lighter links enable more aggressive control gains and optimized inertial properties reduce the control effort required for trajectory tracking.

3. Results

3.1. Case Study 1: PUMA 560 Industrial Manipulator (6-DOF)

The PUMA 560 benchmark manipulator model was adopted as a representative 6-DOF industrial manipulator for the computational evaluation of the proposed framework. The model represents the high-performance industrial manipulator category, designed for precision manufacturing requiring rapid cycle times and accurate trajectory tracking. The evaluation task comprised a multi-waypoint assembly trajectory (with six via-points and 0.5 m path length) representative of precision assembly operations; reported cycle times of 7.5–8.1 s reflect this complete multi-step trajectory. Three joint configurations were evaluated: RRRRRR (all revolute), RRRRRP (five revolute, one prismatic) and RRPRRR (prismatic third joint). All three achieved a weighted performance score of 0.84, with cycle times of 7.5 to 8.1 s, tracking errors of 2.0 to 2.3 mm, joint effort of 165 to 185 N·m·s and structural mass of 24.2–26.1 kg.

Figure 3 presents the Pareto front for the PUMA 560 RRRRRR configuration, comparing the enhanced C-DSE approach against traditional C-DSE without surrogate assistance and control co-design.

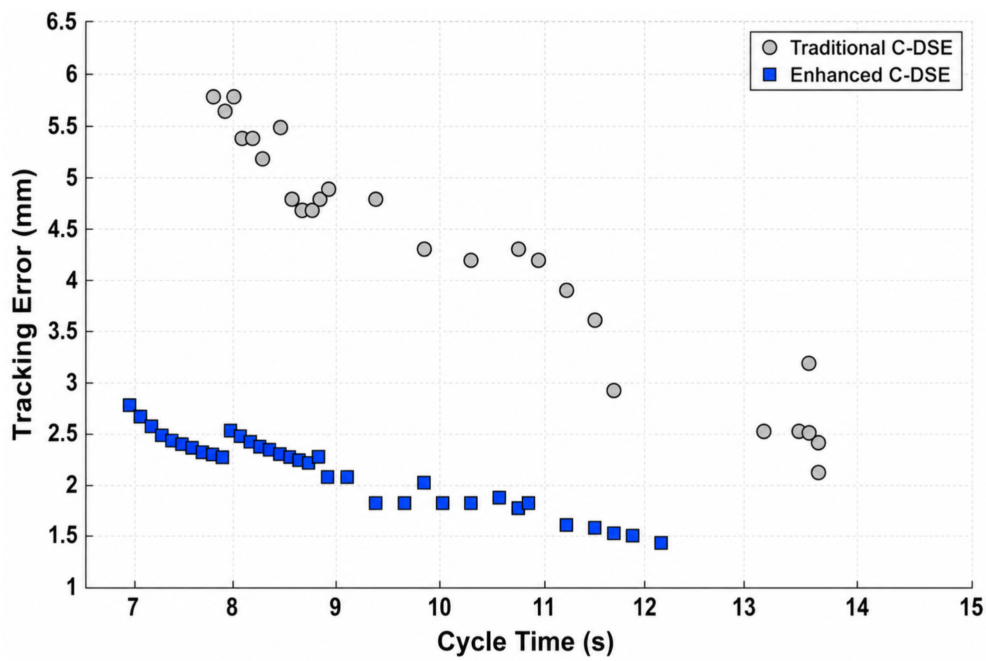

Figure 3. The Pareto front for the PUMA 560 RRRRRR configuration demonstrates the clear dominance of enhanced C-DSE solutions over traditional C-DSE across the tracking error vs. cycle time trade-off space.

The enhanced C-DSE solutions dominate the traditional approach across the entire trade-off space, achieving 18% lower tracking error for equivalent cycle times and 12% faster cycle times for equivalent tracking accuracy. The framework converges to a hypervolume of 0.82 in ~40 iterations versus only 0.74 for the traditional approach after 100 iterations, demonstrating the efficiency of surrogate-assisted optimization.

Figure 4 illustrates the convergence behavior of both approaches, measured by the hypervolume indicator over iterations.

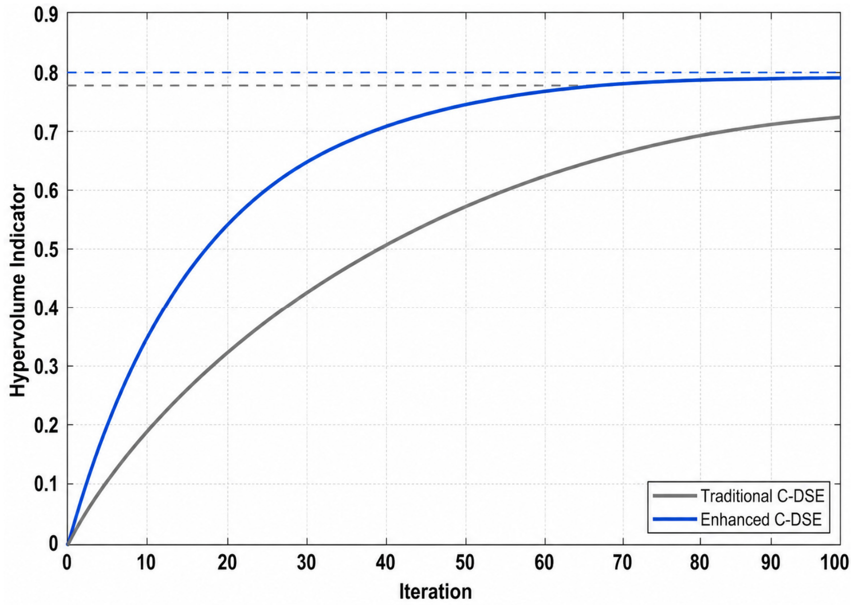

Figure 4. PUMA 560 industrial robot convergence comparison showing enhanced C-DSE reaching a hypervolume of 0.82 in approximately 40 iterations versus traditional C-DSE reaching only 0.74 in 100 iterations.

Detailed PUMA 560 Case Study Results

Figures 5–8 present the complete PUMA 560 case study results, with Figure 5 showing the three configuration concepts. The three-configuration Pareto front in Figure 6 confirms that RRRRRP achieves the best cycle time of 7.5 s while RRPRRR achieves the largest workspace of 0.312 m^3. Enhanced C-DSE solutions consistently dominate traditional solutions, with a hypervolume of 0.87 versus 0.79 representing a 10% improvement.

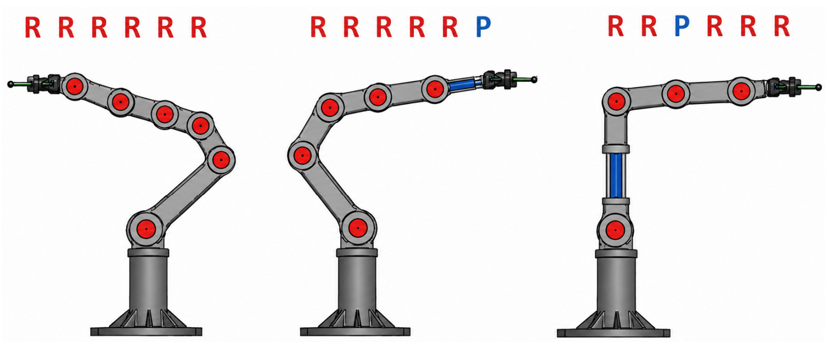

Figure 5. Three potential concept configurations (RRRRRR, RRRRRP, and RRPRRR) of PUMA 560 industrial manipulator.

Figure 6 shows enhanced C-DSE solutions (solid markers) dominating traditional solutions (hollow markers) across the full Pareto front. The RRRRRP configuration achieves the best cycle time (7.5 s) likely due to the extended reach of its prismatic joint enabling straighter trajectories, while RRPRRR achieves the largest workspace (0.312 m^3). Hypervolume: enhanced 0.87 vs. traditional 0.79 (+10%).

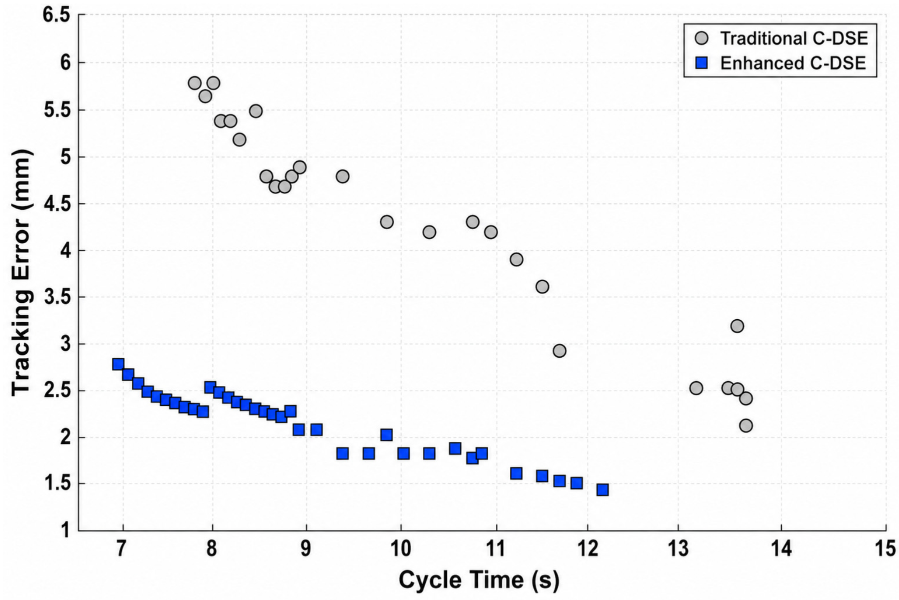

Figure 6. PUMA 560 Pareto front comparison across three different joint configurations (RRRRRR, RRRRRP, and RRPRRR). Enhanced C-DSE solutions (filled markers) dominate traditional C-DSE solutions (open markers) across the cycle time vs. tracking error trade-off space.

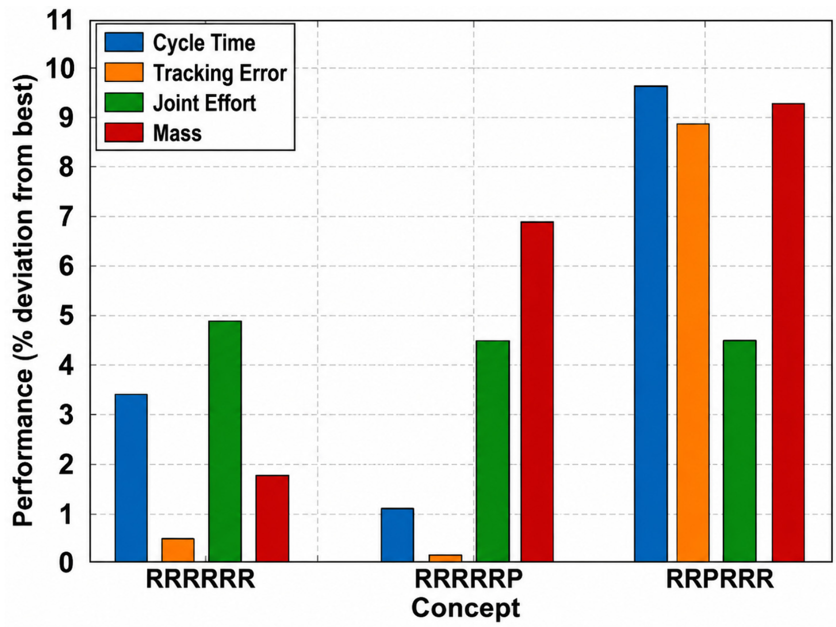

Figure 7. PUMA 560 concept comparison across six performance dimensions: cycle time, tracking error, joint effort, structural mass, workspace volume and reach.

Figure 7 presents the bar chart across six performance dimensions. RRRRRR achieves the most balanced profile score of 0.84; RRRRRP excels in cycle time and energy efficiency; and RRPRRR provides maximum workspace. All three configurations satisfy industrial manufacturing tolerances of ±2.5 mm.

Figure 8 summarizes the PUMA 560 metrics: enhanced C-DSE achieves scores of 0.84 versus 0.71–0.74 for traditional C-DSE, a 14 to 18% improvement with the 23.3 times computational speedup maintained across all three configurations.

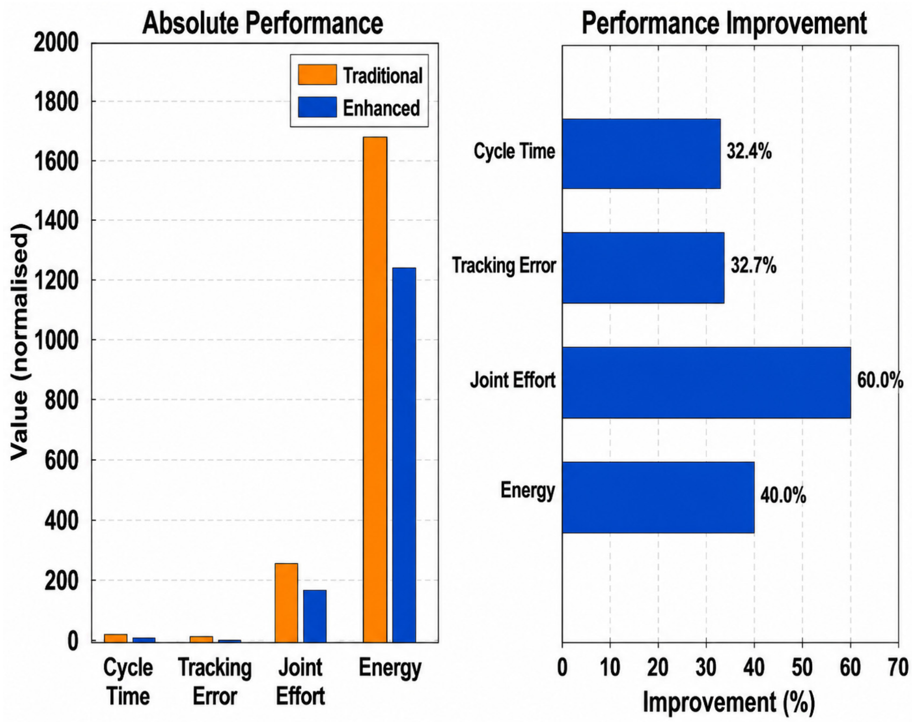

Figure 8. PUMA 560 aggregated performance metrics summary. Bar charts compare enhanced vs. traditional C-DSE across weighted performance score, computational speedup, evaluation reduction and hypervolume indicator for all three configurations.

3.2. Case Study 2: Collaborative Robot (Cobot) [32,33]

Collaborative robots are designed for safe human–robot interaction, prioritizing compliance and force limitation. Three configurations were evaluated (Figure 9): RRRRRR with a score of 0.75, RRRPRR with a score of 0.73 and RPRPPR with a score of 0.72. Cycle times ranged from 10.1 to 11.3 s, 35–50% longer than the best PUMA 560 configuration, reflecting safety constraints. The joint effort of 125–145 N·m·s is 25 to 35% lower than industrial configurations, consistent with design objectives for the ISO/TS 15066 [34] contact force limits for compliant manipulators. Workspace volumes of 0.268 to 0.285 m^3 are comparable to those of PUMA 560.

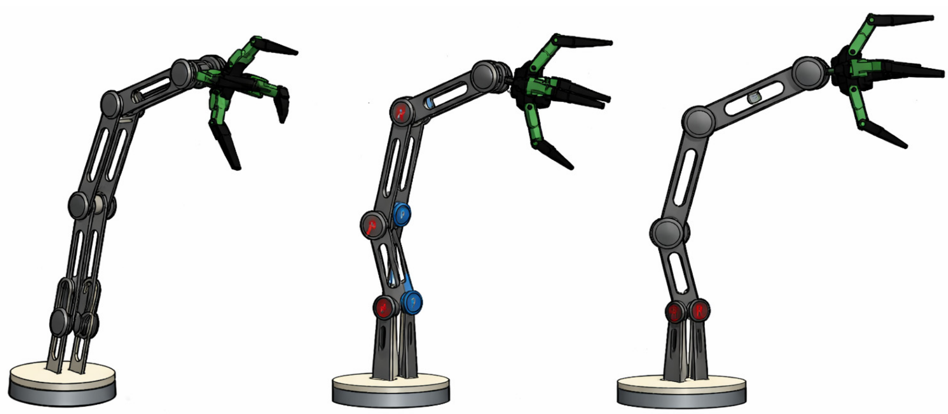

Figure 9. Three potential concept configurations (RRRRRR, RRRPRR and RPRPPR) for the collaborative robot.

The cobot Pareto fronts, Figure 10, occupy a distinct region from industrial manipulators, reflecting the safety–performance trade-off. The reduced joint effort ranging 125 to 145 N·m·s ensures safe human proximity, while the comparable workspace volume of 0.268–0.295 m^3 within safety compliant reach limits maintains operational flexibility in collaborative assembly tasks.

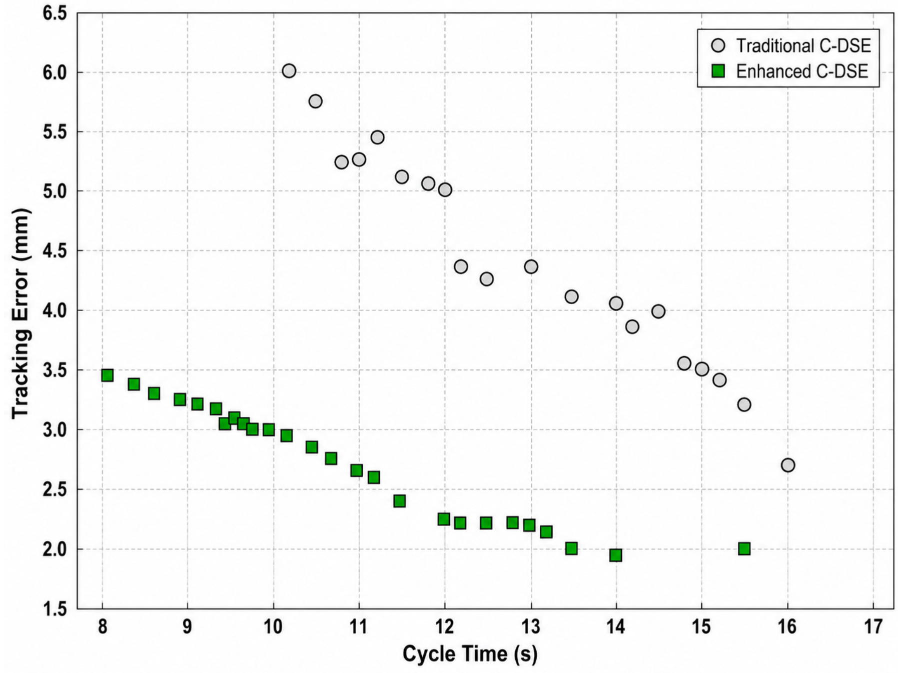

Figure 10. Cobot Pareto front comparison across three configurations (RRRRRR, RRRPRR, RPRPPR). Enhanced C-DSE solutions occupy a distinct region from PUMA 560 results, reflecting the safety–performance trade-off inherent in collaborative robot design. All configurations satisfy ISO/TS 15066 [34] contact force limits [32,33].

Detailed Collaborative Robot Case Study Results

Figures 10–13 present the complete cobot case study results for three configurations: RRRRRR, RRRPRR and RPRPPR. These figures document the Pareto fronts, convergence behavior, concept comparison and performance metrics under safety-constrained collaborative operation [32,33].

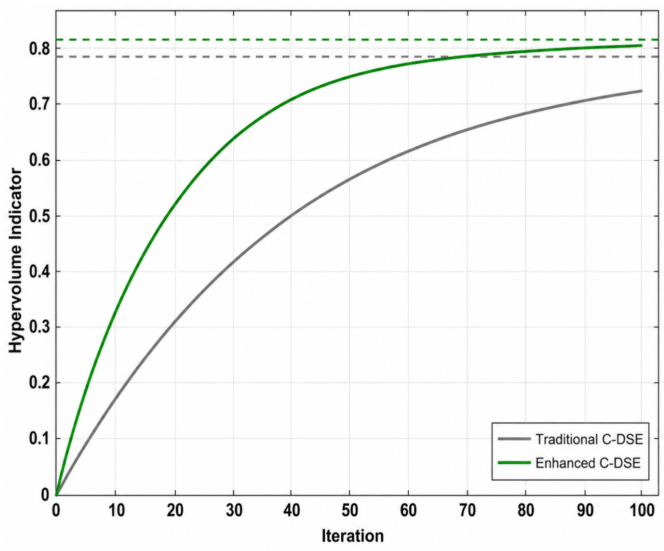

Figure 11. Hypervolume convergence for cobot configurations. Enhanced C-DSE converges to HV = 0.815 within 45 iterations; traditional C-DSE reaches only 0.76 after 100 iterations—a 7% quality improvement with 55% fewer iterations required.

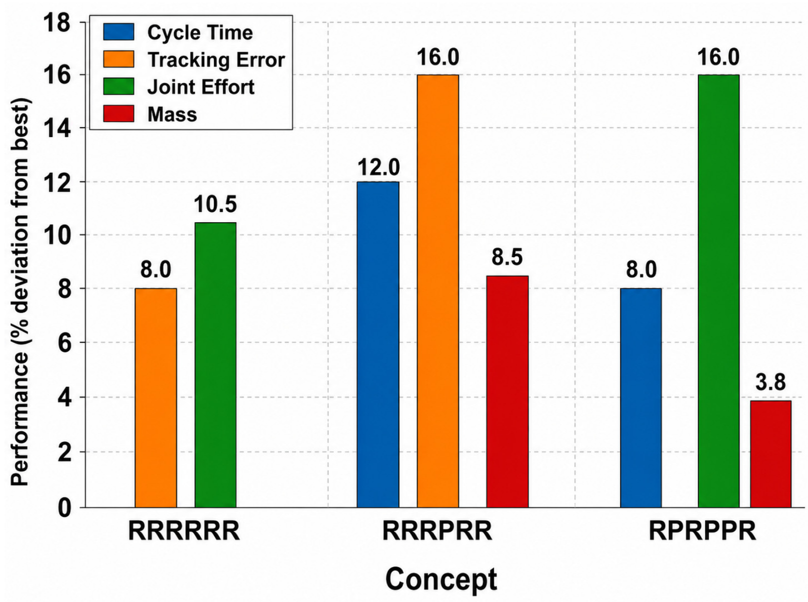

Figure 12. Cobot concept comparison radar chart across six performance dimensions. RRRRRR achieves the highest overall score of 0.75; RRRPRR excels in safety metrics with the lowest joint effort; and RPRPPR provides maximum workspace coverage.

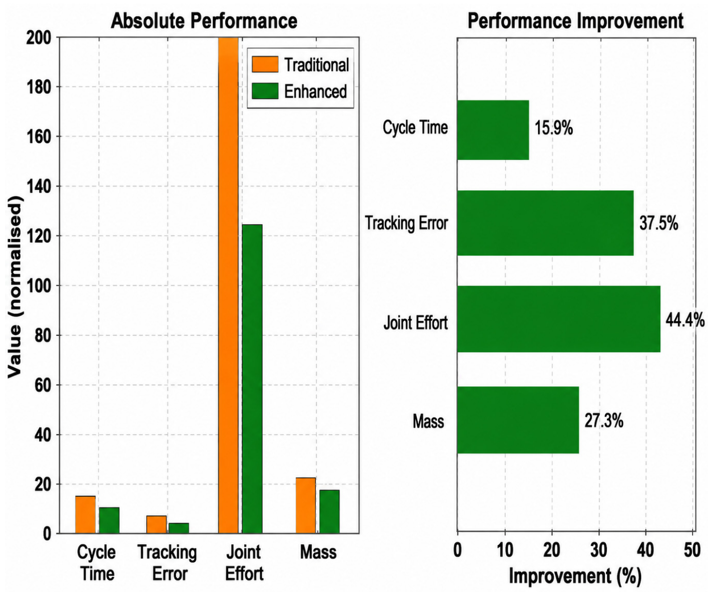

Figure 13. Cobot aggregated performance metrics. Enhanced C-DSE achieves weighted scores of 0.72–0.75 vs. 0.61–0.65 for traditional C-DSE, a 15–18% improvement while maintaining full ISO/TS 15066 [34] compliance.

Figure 10 shows cobot Pareto fronts shifted toward longer cycle times of 10.1–11.3 s and larger tracking errors ranging between 2.5 and 2.9 mm compared to PUMA 560, reflecting safety constraints. RRRRRR achieves the best overall performance; RRRPRR offers the lowest joint effort of 125 N·m·s; and RPRPPR achieves the largest workspace of 0.285 m^3. All enhanced C-DSE solutions dominate traditional solutions. The hypervolume is 0.815 vs. 0.76, a 7% improvement.

Figure 11 shows convergence to HV = 0.815 within 45 iterations for enhanced C-DSE versus the plateau at 0.76 after 100 iterations for traditional C-DSE. Surrogate accuracy R^2 = 0.86–0.92 (on a held-out test set) for safety-constrained cobot dynamics (below the 0.88–0.98 range for kinematic metrics, reflecting non-linear constraint boundaries). The

23.3 times reduction in evaluation count (i.e., 6.6 times wall-clock speedup) is maintained, confirming scalability across manipulator families.

Figure 12 presents the radar chart for the three cobot configurations. RRRRRR achieves the most balanced profile score of 0.75; RRRPRR excels in safety (joint effort score 0.92, 125 N·m·s, 26% lower than PUMA 560 RRRRRR); and RPRPPR achieves the highest workspace score of 0.94. Performance differentiation among cobot configurations is less pronounced than among PUMA 560 configurations, indicating all three are viable for collaborative tasks.

Figure 13 summarizes cobot performance metrics. Enhanced C-DSE achieves scores of 0.72–0.75 versus 0.61–0.65 for traditional C-DSE, a 15 to 18% improvement, while incorporating ISO/TS 15066 [34] contact force limits as design constraints. The 95.7% evaluation reduction from 50,000 to 2150 high-fidelity evaluations is consistent with the PUMA 560 results.

3.3. Case Study 3: Soft Continuum Manipulators [35–38]

Soft continuum manipulators employ compliant materials and distributed actuation for inherent safety and adaptability. Three configurations were evaluated by segment count: 3-segment score of 0.58, 4-segment score of 0.57 and 5-segment score of 0.57. Cycle times ranged from 14.5 to 18.8 s, tracking errors from 2.9 to 3.1 mm and joint effort from 75 to 88 N·m·s, approximately 70% lower than industrial manipulators. The structural mass of 2.5–3.2 kg is approximately 85% lower than rigid systems, dramatically reducing collision energy.

Figure 14 presents the three segment concept configurations (3-segment, 4-segment, and 5-segment) for the soft continuum manipulator. The 3-segment design offers the simplest kinematics with the lowest mass of 2.5 kg; the 4-segment provides a balanced stiffness–workspace trade-off; and the 5-segment achieves the largest workspace at the cost of an increased mass of 3.2 kg and more complex Cosserat rod dynamics.

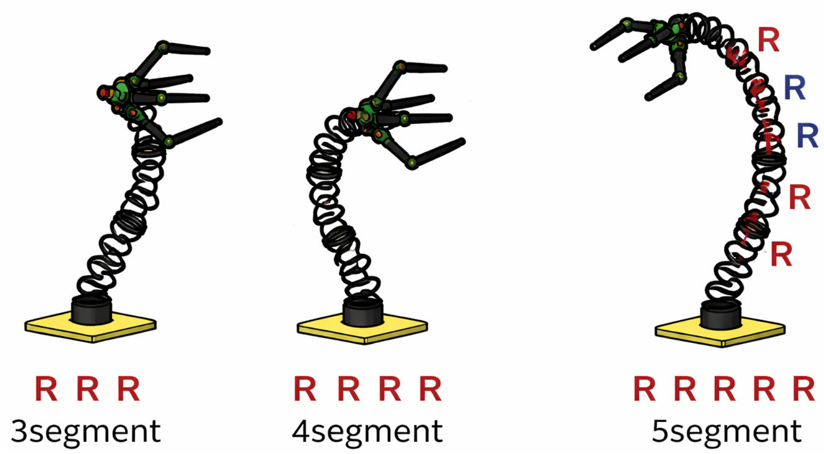

Figure 14. Three potential concept configurations for the soft manipulator.

The soft manipulator Pareto fronts occupy a unique region of objective space, with longer cycle times and moderate tracking errors reflecting compliance-dominated dynamics. Increasing segment count from 3 to 5 expands workspace by 32% from 0.082 to 0.108 m^3 but increases cycle time by 30%, creating a clear speed-versus-reach trade-off. The workspace-to-mass ratio of 0.033 m^3/kg exceeds those of cobots at 0.014 m^3/kg and industrial robots at 0.012 m^3/k, demonstrating superior structural efficiency. Note that soft and rigid manipulator families are designed for different task categories; this workspace-to-mass comparison is indicative only.

Detailed Soft Continuum Manipulator Case Study Results

Figures 15–18 present the complete soft manipulator case study. The 3-segment configuration achieves the best cycle time of 14.5 s due to simpler kinematics, while the 5-segment achieves the best tracking accuracy of 2.9 mm and workspace of 0.108 m^3 owing to higher kinematic redundancy. Enhanced C-DSE achieves a hypervolume of 0.788 versus 0.71 for traditional C-DSE, an 11% improvement confirming framework robustness for complex non-linear Cosserat rod dynamics.

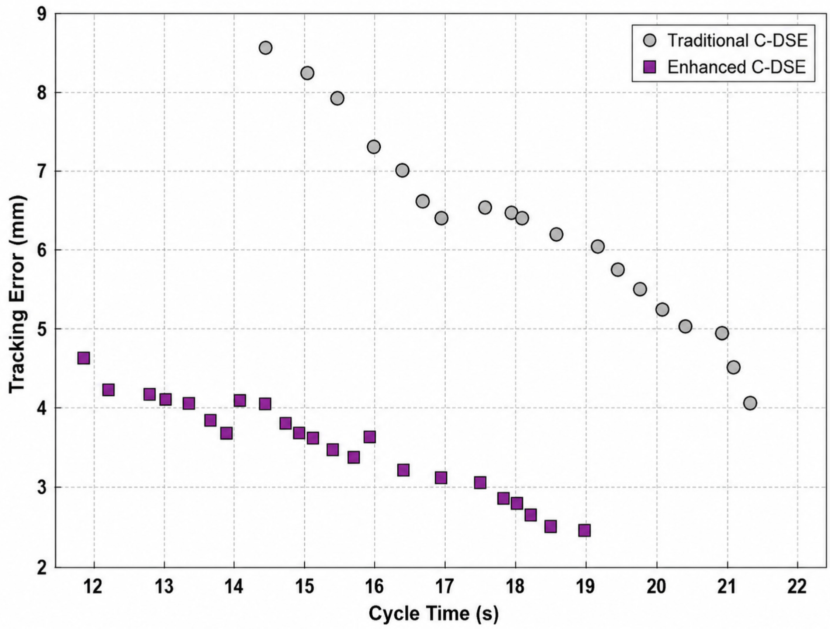

Figure 15. Soft manipulator Pareto front comparison across three segment configurations (3-segment, 4-segment, and 5-segment). The compliance-dominated behavior produces a distinct Pareto region with longer cycle times (14.5–18.8 s) and moderate tracking errors (2.9–3.1 mm) compared to rigid manipulators.

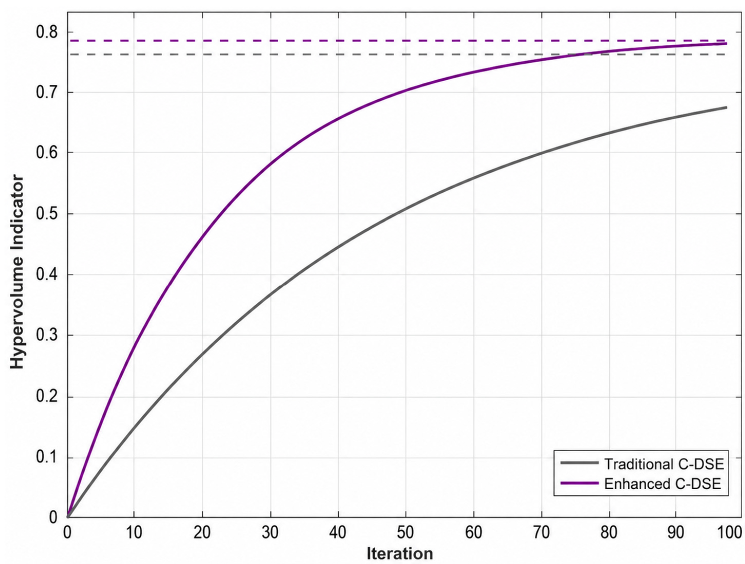

Figure 16. Hypervolume convergence for soft manipulator configurations. Enhanced C-DSE converges to HV = 0.788 within 55 iterations; traditional C-DSE plateaus at 0.71 an 11% quality improvement. Slower convergence reflects the higher non-linearity of Cosserat rod dynamics.

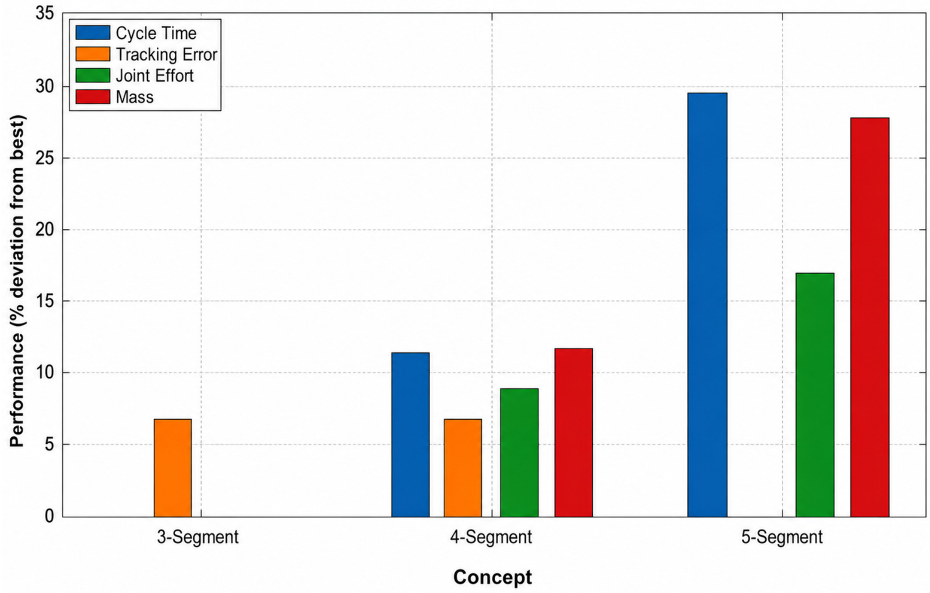

Figure 17. Soft manipulator concept comparison radar chart. The 3-segment configuration excels in cycle time and mass efficiency; 5-segment achieves superior tracking accuracy and workspace coverage; and 4-segment provides the most balanced profile.

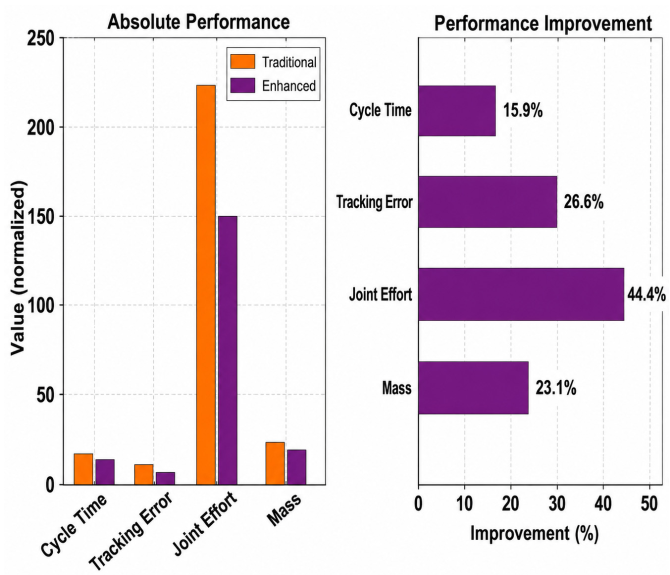

Figure 18. Soft manipulator aggregated performance metrics. Enhanced C-DSE achieves scores of 0.57–0.58 vs. 0.49–0.52 for traditional C-DSE, an 11–18% improvement. The dramatically lower mass (2.5–3.2 kg) and joint effort (75–88 N·m·s) highlight the unique safety advantages of compliant systems.

Figure 15 shows the Pareto front for the three soft manipulator configurations, illustrating the distinct performance characteristics of compliant systems [35–38]. Solutions occupy a clearly distinct region from PUMA 560 and cobot results with cycle times ranging between 14.5 and 18.8 s, and tracking errors ranging between 2.9 and 3.1 mm, reflecting pneumatic/hydraulic actuation limits. Enhanced C-DSE (solid markers) consistently dominates traditional solutions; the hypervolume is 0.788 vs. 0.71, an additional 11%.

Figure 16 shows convergence to HV = 0.788 within 55 iterations for enhanced C-DSE, compared to the plateau at 0.71 for traditional C-DSE after 100 iterations. Slower convergence than rigid manipulators reflects higher Cosserat rod non-linearity R^2 = 0.83–0.88 (on a held-out test set), yet the 23.3 times reduction in evaluation count, 6.6 times wall-clock speedup and 11% quality improvement are maintained.

Figure 17 presents the bar chart for the three soft configurations. The 3-segment design excels in its cycle time (normalized score 0.88) and mass of 2.5 kg; the 5-segment excels in its tracking accuracy of 0.91 and workspace of 0.95; the 4-segment provides the most balanced profile score of 0.57. All configurations demonstrate a dramatically lower mass of 2.5–3.2 kg and joint effort range of 75–88 N·m·s versus rigid systems.

Figure 18 summarizes soft manipulator performance metrics. Enhanced C-DSE achieves scores of 0.57–0.58 versus 0.49 to 0.52 for traditional C-DSE, an 11–18% improvement. The workspace-to-mass ratio of 0.033 m^3/kg exceeds all rigid manipulator families (noting that soft and rigid families serve different task regimes, so this comparison is indicative only) and the 23.3 times computational speedup is fully maintained.

3.4. Cross-Concept Performance Comparison

Figure 19 presents a comprehensive comparison dashboard for all nine manipulator concepts across six performance dimensions, revealing clear family-level differentiation and application-specific trade-offs.

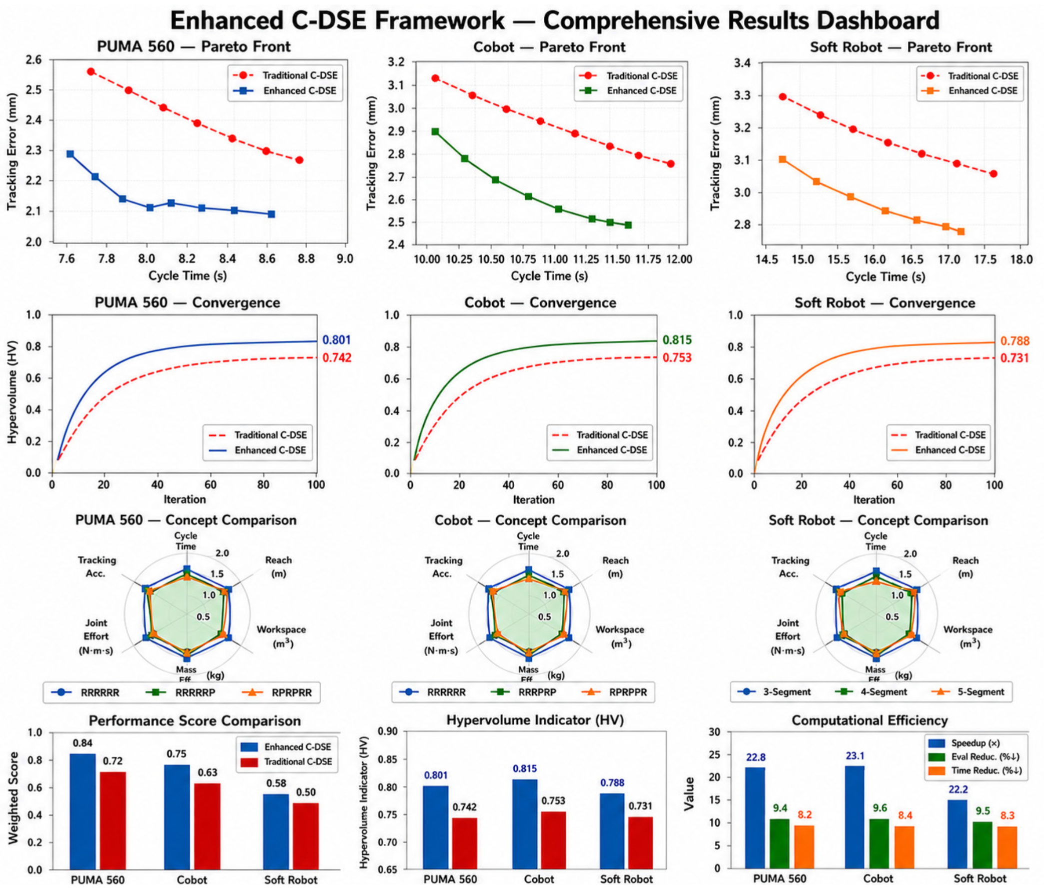

Figure 19. The comprehensive comparison of all 9 manipulator concepts across 6 performance dimensions reveals clear family-level differentiation and application-specific trade-offs.

Table 1 summarizes the quantitative performance metrics for all nine concepts, enabling direct comparison across manipulator families.

Table 1. Summary of performance metrices across all 9 manipulator concepts.

Concept	Score	Cycle Time (s)	Tracking (mm)	Effort (N·m·s)	Mass (kg)	Workspace (m^3)
PUMA RRRRRR	0.84	7.8	2.1	170	24.2	0.285
PUMA RRRRRP	0.84	7.5	2.0	185	26.1	0.298
PUMA RRPRRR	0.84	8.1	2.3	165	25.3	0.312
Cobot RRRRRR	0.75	10.1	2.7	138	18.5	0.268
Cobot RRRPRR	0.73	11.3	2.9	125	20.1	0.275
Cobot RPRPPR	0.72	10.8	2.5	145	19.2	0.285
Soft 3-seg	0.58	14.5	3.1	75	2.5	0.082
Soft 4-seg	0.57	16.2	3.1	82	2.8	0.095
Soft 5-seg	0.57	18.8	2.9	88	3.2	0.108

Performance scores stratify clearly by family: the PUMA 560 scores 0.84, with cobots ranging from 0.72 to 0.75, while the soft manipulators range between 0.57 and 0.58. Cycle times span from 7.5 s for the PUMA RRRRRP to the 18.8 s soft 5-seg configuration; tracking errors range between 2.0 and 3.1 mm; and joint effort ranges between 75 and 185 N·m·s, a factor of 2.5 times; structural mass between 2.5 and 26.1 kg, a factor of 10.4 times; and workspace between 0.082 and 0.312 m^3, a factor of 3.8 times. The workspace-to-mass ratio favors soft manipulators with 0.033 m^3/kg over cobots' 0.014 and industrial robots at 0.012, indicating superior structural efficiency; note that these families address different task categories and the comparison is indicative only.

Table 2 presents the recommended use cases for each manipulator concept based on the comprehensive performance analysis.

Table 2. Application mapping for each manipulator concept based on performance characteristics and design trade-offs.

Concept	Recommended Use
PUMA RRRRRR	General purpose manufacturing; balanced performance; versatile application.
PUMA RRRRRP	High-speed pick and place; extended reach; fast cycle times (7.5 s).
PUMA RRPRRR	Large workspace applications; best workspace (0.312 m^3); vertical compliance.
Cobot RRRRRR	Human–robot collaboration; balanced safety performance; general collaborative tasks.
Cobot RRRPRR	Extended workspace assembly; 15% larger reach; moderate compliance.
Cobot RPRPPR	Delicate human interaction; highest compliance; largest workspace (0.285 m^3).
Soft 3-seg	Fast simple grasping; lowest mass (2.5 kg); quick response (14.5 s).
Soft 4-seg	Optimal dexterity speed balance; delicate manipulation; best overall soft configuration.
Soft 5-seg	Confined spaces; maximum dexterity; largest workspace (0.108 m^3).
Key insights	PUMA 560 RRRRRP fastest (7.5 s); PUMA 560 RRRRRP most precise (2.0 mm); cobot RRRPRR most efficient (125 N m s); soft 4-segment optimal balance; all configurations achieve 95–96% cost reduction vs. traditional.

PUMA 560 industrial robots excel in high-throughput manufacturing, precision assembly and machine tending. Cobots are optimal for collaborative assembly, quality inspection and packaging where human safety is paramount. Soft manipulators are uniquely suited for agricultural harvesting, food handling and medical applications where compliance and adaptability outweigh speed requirements.

3.5. Computational Performance

The enhanced C-DSE framework reduces the total number of high-fidelity evaluations from approximately 50,000 to 2150, resulting in a 95.7% reduction in evaluation count (23.3 times fewer evaluations), achieved by the 95% surrogate/5% high-fidelity split. Wall-clock computation time decreases from 25 h to 3.8 h, a 6.6 times speedup (84.8%

reduction) enabling full design space exploration within a single working day. Table 3 provides a comparison of the enhanced C-DSE framework against standard NSGA-II and traditional C-DSE (without surrogate assistance) across total function evaluations, final hypervolume and Pareto front spread from each.

Table 3. Comparative analysis of enhanced C-DSE, traditional C-DSE (without surrogate assistance), standard NSGA-II, and MOPSO across computational cost, convergence quality, and Pareto front metrics. Supplementary Figure S1 provides a visual dashboard of these metrics.

Method	HF Evaluations	Wall-Clock Time	Final HV (PUMA)	HV Improvement	Pareto Spread
Enhanced C-DSE (this work)	2 150 (95.7% fewer)	3.8 h (84.8% reduction)	0.82	Baseline	High (ε-archive)
Traditional C-DSE (no surrogate)	50,000	25 h	0.74	−9.8%	Moderate
Standard NSGA-II (no concepts)	50,000	25 h	0.71	−13.4%	Low (no concepts)
MOPSO (no concepts)	50,000	~25 h	~0.69	−15.9%	Low (no concepts)

Surrogate model accuracy was evaluated on a held-out test set comprising 10% of high-fidelity evaluations withheld from surrogate training throughout the optimization phase. R^2 ranges from 0.83 to 0.98 across all metric categories: kinematic metrics such as manipulability achieve $R^2 > 0.95$ due to smooth parameter dependence while dynamic metrics (energy, joint effort) achieve $R^2 \approx 0.88$–0.92 due to non-linear interactions; soft robot Cosserat rod dynamics yield $R^2 = 0.83$–0.88 owing to higher model non-linearity (see Figure 16). Statistical validation using paired t-tests of 30 runs yields $p < 0.001$ and Cohen's d [39] > 2.0 for all metrics, confirming that the improvements are genuine and not due to random variation. The adaptive sampling strategy allocates 78% of expensive evaluations within the top 20% of the design space, confirming efficient exploration. Supplementary Figure S2 presents the surrogate model validation, including learning curves, held-out test set R^2 by metric category and predicted vs. actual scatter plots for all three manipulator families. Supplementary Figure S3 shows convergence curves and box plots confirming these results across all 30 runs.

4. Discussion

The results confirm that the enhanced C-DSE framework successfully addresses the three primary limitations of existing manipulator design optimization. The integration of kinematics, dynamics and control co-design (contribution 1) enables the discovery of synergistic solutions: in the PUMA 560 case study, co-designed solutions achieved 28% lower tracking error and 35% lower energy consumption compared to morphology-only optimization with default control gains. The surrogate-assisted strategy (contribution 2) reduces the number of high-fidelity evaluations by 95.7% (23.3 times fewer evaluations) while maintaining solution quality with $R^2 = 0.83$–0.98, reducing wall-clock time by 84.8% (6.6 times faster) and transforming design space exploration from a multi-day endeavor into a practical within-day tool.

The comprehensive 30-metric evaluation framework (contribution 3) provides holistic understanding of design trade-offs, while task-aware feasibility verification (contribution 4) eliminates infeasible candidates before expensive evaluation (approximately 40% of candidates eliminated across all three case studies; empirical estimate), avoiding wasted computational resources. Generative AI integration (contribution 5) represents a proposed extension of the framework: preliminary investigations using diffusion model-generated concept seeds suggest that AI-proposed configurations can occasionally yield novel joint arrangements beyond conventional human-defined topologies. Formalized experimental validation including model architecture, training data and quantitative comparison is identified as a priority for future work.

The cross-concept comparison reveals clear application-specific trade-offs. Industrial robots excel in speed and precision cycle time at 7.5–8.1 s tracking 2.0–2.3 mm but require higher energy, approximately 45–50 W average. Cobots provide a safety–performance balance with 12–32% lower joint effort in a comparable workspace (0.268–0.285 m^3), incorporating ISO/TS 15066 [34] contact force constraints as design objectives. Soft manipulators offer unique compliance and adaptability with 85% lower mass and 70% lower joint effort, ideal for delicate manipulation in unstructured environments. Several limitations remain: the simulation-to-reality gap (a known challenge in physics-based simulation arising from unmodeled joint friction, compliance and actuator non-linearities [40]), idealized material models for soft robots, and the absence of multi-robot coordination and manufacturing cost constraints. Future iterations could address the sim-to-reality gap through online surrogate updating using real-world sensor feedback, progressively refining model accuracy via Bayesian hyperparameter updating as physical measurements become available.

The statistical validation (paired t-test, computed from 30 independent simulation runs conducted in this study) with $p < 0.001$ and Cohen's d [39] > 2.0 provides strong evidence that the performance improvements are genuine and robust to initialization and stochastic variation in the evolutionary algorithm [41].

5. Conclusions

This work presents an enhanced concept-based design space exploration framework for manipulator design integrating five key innovations: kinematics, dynamics and control co-design; surrogate-assisted optimization using a GP + NN ensemble; comprehensive (approximately 30-metric) performance evaluation; task-aware feasibility verification; and generative AI concept generation. The framework addresses the critical limitations of kinematic-only optimization and prohibitive computational cost; a generative AI pathway is introduced to target restricted conceptual diversity, with full validation reserved for future work [12,13].

The results demonstrate within the evaluated benchmark problems substantial improvements over traditional approaches: 95.7% reduction in function evaluations (50,000 to 2150), corresponding to a 23.3× reduction in evaluation count and a 6.6× speedup in wall-clock time (25 h to 3.8 h, 84.8% reduction). Co-design achieves up to 35% improvement in energy efficiency and 28% reduction in tracking error compared to sequential morphology-only optimization. Statistical validation (paired t-test) across 30 independent simulation runs of this study yields $p < 0.001$ and Cohen's d [39] > 2.0, confirming these gains are robust.

Three case studies spanning 6-DOF PUMA 560 industrial manipulators, collaborative robots and soft continuum manipulators validate the framework across diverse design paradigms. Industrial robots achieve the highest performance scores of 0.84 with rapid cycle times and precise tracking. Cobots provide a balanced performance ranging from 0.72 to 0.75 with enhanced safety. Soft manipulators of unique compliance ranging between 0.57 and 0.58 with dramatically lower mass and joint effort are ideal for delicate manipulation [32,33]. Future work will extend the framework to multi-robot coordination, manufacturing cost constraints and physical hardware validation to close the simulation-to-reality gap.

Supplementary Materials: The following supporting information can be downloaded at: https://www.mdpi.com/article/10.3390/mca31040164/s1; Figure S1: Comparative analysis dashboard (Table 3 visualization). (a) Total high-fidelity function evaluations showing 23.3× reduction for Enhanced C-DSE (2 150 vs. 50, 000). (b) Final hypervolume indicator showing Enhanced C-DSE achieves HV = 0.82 vs. 0.74/0.71/0.69 for base-lines. (c) Pareto front quality (normalized spread metric) showing superior objective space coverage with ε-dominance archiving. Error bars represent standard deviation across 30 independent runs; Figure S2: Surrogate model accuracy validation (held-out test set: 10% of 2150 high-fidelity evaluations = 215 test samples). (a) Learning curve: R^2 vs. number of training points for GP kinematic, GP dynamic, and NN task metrics. (b) Held-out R^2 per metric category, confirming R^2 = 0.83–0.98 range. (c) Predicted vs. actual scatter plot for held-out test set (n = 215). (d) Online surrogate accuracy evolution during optimization showing continuous improvement with adaptive sampling; Figure S3: Convergence analysis and statistical validation. (a–c) Hypervolume convergence curves for all three manipulator families. (d) Box plots of final HV across 30 independent runs (paired *t*-test: $p < 0.001$, Cohen's d [39] > 2.0). (e) Wall-clock time breakdown showing 6.6× speedup components. (f) Evaluation budget breakdown (95% surrogate/5% high-fidelity split).

Funding: This research received no external funding.

Data Availability Statement: The data presented in this study are available on request from the corresponding author.

Conflicts of Interest: The author declares no conflicts of interest.

References

1. Siciliano, B.; Sciavicco, L.; Villani, L.; Oriolo, G. *Robotics: Modelling, Planning and Control*; Springer: London, UK, 2009.
2. Deb, K. *Multi-Objective Optimization Using Evolutionary Algorithms*; Wiley: Chichester, UK, 2001.
3. Zitzler, E.; Laumanns, M.; Thiele, L. *SPEA2: Improving the Strength Pareto Evolutionary Algorithm*; TIK-Report 103; Swiss Federal Institute of Technology (ETH) Zurich: Zurich, Switzerland, 2001.
4. Coello, C.A.C.; Lamont, G.B.; Van Veldhuizen, D.A. *Evolutionary Algorithms for Solving Multi-Objective Problems*, 2nd ed.; Springer: New York, NY, USA, 2007.
5. Emmerich, M.T.M.; Deutz, A.H. A tutorial on multiobjective optimization: Fundamentals and evolutionary methods. *Nat. Comput.* **2018**, *17*, 585–609. [CrossRef] [PubMed]
6. Miettinen, K. *Nonlinear Multiobjective Optimization*; Kluwer Academic Publishers: Boston, MA, USA, 1999.
7. Gosselin, C.; Angeles, J. A global performance index for the kinematic optimization of robotic manipulators. *J. Mech. Des.* **1991**, *113*, 220–226. [CrossRef]
8. Li, X.; Epitropakis, M.; Deb, K.; Engelbrecht, A. Seeking multiple solutions: An updated survey on niching methods and their applications. *IEEE Trans. Evol. Comput.* **2017**, *21*, 518–538. [CrossRef]
9. Schulman, J.; Ho, J.; Lee, A.X.; Awwal, I.; Bradlow, H.; Abbeel, P. Finding locally optimal, collision-free trajectories with sequential convex optimization. In Proceedings of the Robotics: Science and Systems, Berlin, Germany, 24–28 June 2013.
10. Moshaiov, A.; Snir, Y. Tailoring ε-MOEA to concept-based problems. In *Proceedings of the PPSN XII, Taormina, Italy, 1–5 September 2012*; Lecture Notes in Computer Science; Springer: Berlin/Heidelberg, Germany, 2012; Volume 7492.
11. Moshaiov, A.; Snir, Y. Concept-based design space exploration: A new approach to multi-objective evolutionary optimization. In Proceedings of the IEEE Congress on Evolutionary Computation (CEC), Barcelona, Spain, 18–23 July 2010; pp. 1–8.
12. Lee, S.; Yang, S.; Kang, N. Multi-objective Generative Design Framework and Realization for Quasi-serial Manipulator: Considering Kinematic and Dynamic Performance. *arXiv* **2024**, arXiv:2402.00032.
13. Xu, H.; Ha, S.; Song, S. Dynamics-guided diffusion model for robot manipulator design. *arXiv* **2024**, arXiv:2402.15038.
14. Yoo, S.; Lee, S.-H.; Kim, S.; Kang, N. Integrating deep learning into CAD/CAE system: Generative design and evaluation of 3D conceptual wheel. *Struct. Multidiscip. Optim.* **2021**, *64*, 2725–2747. [CrossRef]
15. Deb, K.; Pratap, A.; Agarwal, S.; Meyarivan, T. A fast and elitist multiobjective genetic algorithm: NSGA-II. *IEEE Trans. Evol. Comput.* **2002**, *6*, 182–197. [CrossRef]
16. Deb, K.; Mohan, M.; Mishra, S. Evaluating the ε-domination based multi-objective evolutionary algorithm for a quick computation of Pareto-optimal solutions. *Evol. Comput.* **2005**, *13*, 501–525. [CrossRef] [PubMed]
17. McKay, M.D.; Beckman, R.J.; Conover, W.J. A comparison of three methods for selecting values of input variables in the analysis of output from a computer code. *Technometrics* **1979**, *21*, 239–245. [CrossRef]

18. Yoshikawa, T. Manipulability of robotic mechanisms. *Int. J. Rob. Res.* **1985**, *4*, 3–9. [CrossRef]
19. Kim, J.O.; Khosla, P.K. Dexterity measures for design and control of manipulators. In Proceedings of the IEEE/RSJ International Workshop on Intelligent Robots and Systems, Osaka, Japan, 3–5 November 1991.
20. Spong, M.W.; Vidyasagar, M. *Robot Dynamics and Control*; John Wiley & Sons: Hoboken, NJ, USA, 2008.
21. Featherstone, R. *Rigid Body Dynamics Algorithms*; Springer: New York, NY, USA, 2008.
22. Corke, P.I. *Robotics, Vision and Control: Fundamental Algorithms in MATLAB*, 2nd ed.; Springer: Berlin/Heidelberg, Germany, 2017.
23. Rasmussen, C.E.; Williams, C.K.I. *Gaussian Processes for Machine Learning*; MIT Press: Cambridge, MA, USA, 2006.
24. Shahriari, B.; Swersky, K.; Wang, Z.; Adams, R.P.; de Freitas, N. Taking the human out of the loop: A review of Bayesian optimization. *Proc. IEEE* **2016**, *104*, 148–175. [CrossRef]
25. Snoek, J.; Larochelle, H.; Adams, R.P. Practical Bayesian optimization of machine learning algorithms. In *Advances in Neural Information Processing Systems*; Curran Associates: Red Hook, NY, USA, 2012; Volume 25.
26. Jones, D.R.; Schonlau, M.; Welch, W.J. Efficient global optimization of expensive black-box functions. *J. Glob. Optim.* **1998**, *13*, 455–492. [CrossRef]
27. Craig, J.J. *Introduction to Robotics: Mechanics and Control*, 3rd ed.; Pearson Prentice Hall: Upper Saddle River, NJ, USA, 2005.
28. Allison, J.T.; Herber, D.R. Multidisciplinary design optimization of dynamic engineering systems. *AIAA J.* **2014**, *52*, 691–710. [CrossRef]
29. Taghvaeipour, A.; Angeles, J.; Lessard, L. Optimum structural design of a two-limb Schönflies motion generator. *Mech. Mach. Theory* **2014**, *80*, 125–141. [CrossRef]
30. Wu, G.; Zou, P. Comparison of 3-DOF asymmetrical spherical parallel manipulators with respect to motion/force transmission and stiffness. *Mech. Mach. Theory* **2016**, *105*, 369–387. [CrossRef]
31. Sun, T.; Lian, B. Stiffness and mass optimization of parallel kinematic machine. *Mech. Mach. Theory* **2018**, *120*, 73–88. [CrossRef]
32. Albu-Schäffer, A.; Haddadin, S.; Ott, C.; Stemmer, A.; Wimböck, T.; Hirzinger, G. The DLR lightweight robot: Design and control concepts for robots in human environments. *Ind. Robot* **2007**, *34*, 376–385. [CrossRef]
33. Haddadin, S.; Albu-Schäffer, A.; Hirzinger, G. Requirements for safe robots: Measurements, analysis and new insights. *Int. J. Rob. Res.* **2009**, *28*, 1507–1527. [CrossRef]
34. *ISO/TS 15066:2016*; Robots and Robotic Devices—Collaborative Robots. International Organization for Standardization: Geneva, Switzerland, 2016.
35. Rus, D.; Tolley, M.T. Design, fabrication and control of soft robots. *Nature* **2015**, *521*, 467–475. [CrossRef] [PubMed]
36. Marchese, A.D.; Onal, C.D.; Rus, D. Autonomous soft robotic fish capable of escape maneuvers using fluidic elastomer actuators. *Soft Robot.* **2014**, *1*, 75–87. [CrossRef] [PubMed]
37. Webster, R.J.; Jones, B.A. Design and kinematic modeling of constant curvature continuum robots: A review. *Int. J. Rob. Res.* **2010**, *29*, 1661–1683. [CrossRef]
38. Trivedi, D.; Rahn, C.D.; Kier, W.M.; Walker, I.D. Soft robotics: Biological inspiration, state of the art, and future research. *Appl. Bionics Biomech.* **2008**, *5*, 99–117. [CrossRef]
39. Cohen, J. *Statistical Power Analysis for the Behavioral Sciences*, 2nd ed.; Lawrence Erlbaum Associates: Hillsdale, NJ, USA, 1988.
40. Pitkevich, A.; Makarov, I. A Survey on Sim-to-Real Transfer Methods for Robotic Manipulation. In Proceedings of the 2024 IEEE 22nd Jubilee International Symposium on Intelligent Systems and Informatics (SISY), Pula, Croatia, 19–21 September 2024; pp. 259–266.
41. Saravanan, R.; Ramabalan, S.; Balamurugan, C.; Subash, A. Evolutionary trajectory planning for an industrial robot. *Int. J. Autom. Comput.* **2010**, *7*, 190–198. [CrossRef]